analytical chemistry

pubs.acs.org/ac Article

Target-Activating and Toehold Displacement Ag NCs/GO Biosensor-Mediating Signal Shift and Enhancement for Simultaneous Multiple Detection

Da-Qian Feng and Guoliang Liu*

Cite This: *Anal. Chem.* 2021, 93, 16025−16034 Read Online

ACCESS | Metrics & More | Article Recommendations | Supporting Information

ABSTRACT: Herein, we demonstrate that a new multicolor silver nanoclusters/graphene oxide (Ag NCs/GO) hybrid material, upon target response, undergoes a configuration transformation, based on entropy-driven enzyme-free toehold-mediated strand displacement reaction, achieving emission shift and enhancement. To realize the aim above, two different synthesis routes (route I and II) of synthesizing fluorescent Ag NCs for constructing toehold displacement Ag NCs/GO biosensor is designed and performed. Influenza A virus subtype genes (H1N1 and H5N1) as a model can efficiently initiate the operation of entropy-driven displacement reaction, resulting in activatable fluorescence. Red-emitting and green-emitting Ag NCs tethering the complementary sequence of H1N1 (pDNA1) and H5N1 (pDNA2) are indirectly immobilized on GO surface through binding with capture DNA (cDNA1 and cDNA2), respectively, forming multicolor pDNA-Ag NCs/GO nanohybrid materials. However, they do not exhibit nearly fluorescence signals attributed to energy transfer from donor Ag NCs to acceptor GO. Upon adding targets H1N1 and H5N1 (tDNA1 and tDNA2), pDNA1-Ag NCs and pDNA2-Ag NCs detach from GO, based on toehold-mediated strand displacement reaction, which interferes the energy transfer and leads to significant fluorescence enhancement. More interestingly, the activatable process is accompanied by remarkable hypsochromic shift (19 nm) or bathochromic shift (21 nm) emission with quite high fluorescence recovery rates (823.35% and 693.62%). Therefore, based on these phenomena, a novel multiple approach has been developed with the assistance of toehold displacement and Ag NCs/GO nanohybrid materials. As for the remarkable emission recovery and multichannel signal, the proposed approach displays the promising application prospect in accurate diagnosis and treatment.

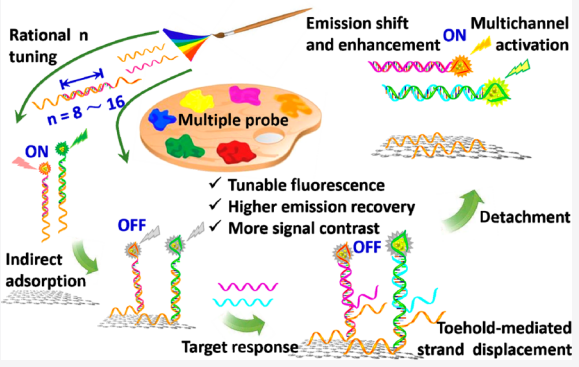

INTRODUCTION

Activatable fluorescence probes are attracting increasing attention among different research fields, because it effectively overcomes the inevitable defects of traditional quenched fluorescent sensors, such as false positive response from various environmental factors and the interference of background signal from unbound probes.[1−4] The ideal activation probe should possess the following characteristic that it only exhibits the remarkably enhanced fluorescence signal upon the addition of the analyte, while it does not appear nearly fluorescence in the absence of the analyte.[5,6] The reported activatable fluorescent probes are mostly constructed based on the strategy of enzyme cleavage of the linker, including the peptide or polymer.[7−9] The opposite ends of the linker are attached to a fluorophore and a quencher, respectively. However, searching specific cancer-related enzyme is difficult and nonversatile, which greatly restricts the application range of this strategy. Moreover, it is quite difficult to achieve real-time and continuous tracking, because the fluorophore detaches from the probe, according to the above principle. Developing a new strategy for constructing activatable fluorescent probes would be an exciting and challenging study.

Until now, different nanomaterials including gold nanoparticles, manganese dioxide nanosheet, metal−organic frameworks, and carbon nanomaterials have been chosen as efficient fluorescence quenchers.[10−14] Especially, graphene oxide (GO) is applied for biosensor fabrication and as a drug delivery vehicle, because of its unique structure property of consisting of two-dimensional sheets that are atomically thin. Besides, GO has high affinity for single-stranded DNA (ssDNA) via noncovalent hydrophobic and $\pi-\pi$ stacking interactions, but GO only possesses a very low affinity for double-stranded DNA (dsDNA).[15] These properties make GO as the promising

Received: August 19, 2021
Accepted: November 15, 2021
Published: November 24, 2021

fluorescence quencher in the construction of activatable probes without requiring covalent attachment to the probe. Following this assumption, GO can bind and quench a fluorescent dye-labeled ssDNA (F-ssDNA). In contrast, the addition of the target can competitively combine with F-ssDNA and disturbs the interaction between the F-ssDNA and GO, leading to the significant restoration of quenched fluorescence of the fluorophore. On the basis of this principle, a variety of biosensors have been established.[16−18] However, the existing reported methods are mostly established based on direct adsorption of the F-ssDNA on the GO in which nonspecific strand displacement occurs by noncomplementary ssDNA, seriously disturbing and lowering the sensitivity of the probe.

Generally speaking, fluorescent organic dyes and semiconductor quantum dots are usually chosen as the fluorescent labeling groups tethering to the end of ssDNA, forming F-ssDNA. However, these fluorophores have intrinsic weaknesses, such as particle sizes that are too large, photobleaching, low biocompatibility, and toxicity. Fluorescent noble-metal nanoclusters, especially ssDNA templated silver nanoclusters (ssDNA-Ag NCs), as a new type of fluorescence nanomaterials, arouse great interest among researchers in various fields, because of its unique properties, including ultrasmall size, low toxicity, good photostability, excellent biocompatibility, and tunable emission wavelength.[19,20] These features make ssDNA-Ag NCs an attractive alternative for conventional fluorophores such as fluorescent organic dyes and semiconductor quantum dots.[21] Moreover, ssDNA-Ag NCs, possessing programmable and flexible design, and facilely functional modification advantages, would be an ideal reporter element for developing toehold displacement Ag NCs/GO biosensor.

To address the potential issues described above, an activatable multiplexed sensor is established by employing ssDNA-Ag NCs as the energy donor and using GO as the energy acceptor, based on the toehold-mediated strand displacement mechanism in this study (Scheme 1). Toehold-

Scheme 1. Schematic Illustration of the Indirect Adsorption pDNA-Ag NCs/GO Nanohybrid Materials for Multiple Detection Based on Toehold-Mediated Strand Displacement Reaction

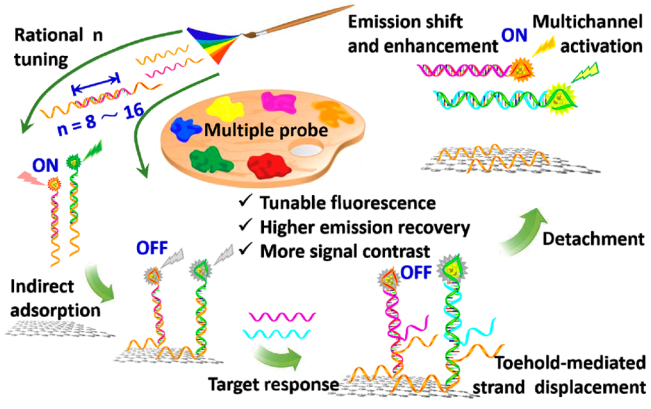

mediated DNA strand displacement reaction refers to a strand displacement reaction of the hybridized dsDNA driven by a toehold domain, leading to a subsequent branch migration.[22−27] Because of its intrinsic nature of the high sequence selectivity, it may address the weakness of nonspecific strand displacement of fluorescent dye-labeled ssDNA/GO-based direct adsorption probe. As the proof of concept, the biomarker Influenza A virus gene (tDNA) is chosen as the target model to initiate the operation of entropy-driven displacement reaction and leads to activatable fluorescence. Nondirect adsorption strategy of ssDNA-based probe on the GO is adopted for the further assay. In order to achieve the aim, probe DNA (pDNA) and capture DNA (cDNA) are designed. The pDNA consists of prepared fluorescent ssDNA-Ag NCs conjugating the complementary sequence of tDNA, while cDNA is composed of a partial fragment of tDNA tethering poly adenine nucleosides (A_{20}) tail (see the Experimental Section and Scheme S1 in the Supporting Information). Two different synthesized routes are performed. The pDNA1 is first incubated with cDNA1(n) to form partial complementary duplex-stranded fragment, which is then chosen as the scaffold for synthesizing red-emitting Ag NCs in situ (Scheme 2, Route I). Meanwhile, pDNA1 is selected for

Scheme 2. Schematic Representation of Two Different Synthesis Routes (Route I and II) of Synthesizing Fluorescent Ag NCs for Constructing Activatable Toehold Displacement Ag NCs/GO Biosensor[a]

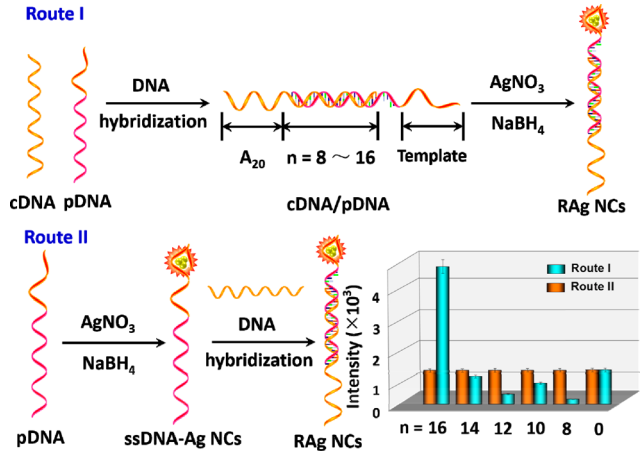

[a]The inserted histogram is the histogram of fluorescence intensity at maximum emission wavelength under different values of n (the cyan represents route I while the orange represents the route II).

synthesizing red-emitting Ag NCs before the incubation with cDNA1 (Scheme 2, Route II). The probe (pDNA-Ag NCs) is indirectly immobilized on the GO surface through the double-stranded region of its hybridization with a cDNA fragment. As for the high affinity of A_{20} tail to the GO, the pDNA-Ag NCs/cDNA(16) duplex is indirectly adsorbed on the GO surface, forming pDNA/cDNA(16)-Ag NCs/GO nanohybrid materials, then leading to quenching fluorescence signal due to energy transfer, which is called the "OFF" state. The presence of target H1N1 and H5N1 can effectively initiate the entropy-driven toehold-mediated strand displacement reaction and form a probe-target duplex-stranded structure, resulting in the departure of the pDNA-Ag NCs from the GO surface and the disturbance of the energy transfer process, which generates a remarkably enhanced fluorescence signal, named as "ON" state. Interestingly, the fluorescence activation is accompanied by the significant hypsochromic shift (19 nm) for RpDNA1-Ag NCs while bathochromic shift (21 nm) for GpDNA2-Ag NCs, called chemopalette (Scheme 2, Route II). The tunable fluorescence properties of pDNA-Ag NCs enable the multi-

https://doi.org/10.1021/acs.analchem.1c03570
Anal. Chem. 2021, 93, 16025−16034

plexed determination of virus subtype genes H1N1 and H5N1 simultaneously. The new strategy of constructing activatable fluorescence Ag NCs/GO-based probe combines with toehold-mediated strand displacement mechanism, which possesses great potential to be applied as a power tool for biomolecule analysis and clinical disease diagnosis. This unique design provides a new avenue for modulating emission wavelength and intensity of Ag NCs without changing the bases of the template and also extends the application of toehold displacement.

EXPERIMENTAL SECTION

Materials. The graphene oxide (GO) dissolved in ultrapure water (5 mg/mL) was purchased from Nanjing Ji Cang Nano Tech Co., Ltd. (Nanjing, China) and used without further processing. Sodium borohydride ($NaBH_4$, 98%) and silver nitrate ($AgNO_3$, 99.99%) were purchased from Alfa Aesar and used without further purification. All other reagents were all of analytical grade and used as received without further purification. All oligonucleotides were HPLC-purified and freeze-dried by the supplier (Sangon Biotech Co., Ltd., Shanghai, China). The oligonucleotides were used as provided and dissolved in an ultrapure water to obtain stock solutions (100 μM). All solutions were prepared with Millipore Milli-Q ultrapure water (18.2 MΩ cm). A phosphate buffer solution (20 mM, pH 7.0) was used to control the acidity of the reaction. The oligonucleotide sequences used in this study are listed as follows:

(**1**) 5'-CCTCCTTCCTCCTTCTTCATCGAGAGTGTAGTCG-3' (pDNA1)

(**2**) 5'-CGACTACACTCTCGATGAAGAA-3' (H1N1, tDNA1)

(**3**) 5'-A_{20}-CGACTACACTCTCGAT-3' (cDNA1(n16))

(**4**) 5'-A_{20}-CGACTACACTCTCG-3' (cDNA1(n14))

(**5**) 5'-A_{20}-CGACTACACTCT-3' (cDNA1(n12))

(**6**) 5'-A_{20}-CGACTACACT-3' (cDNA1(n10)

(**7**) 5'-A_{20}-CGACTACA-3' (cDNA1(n8))

(**8**) 5'-AAAAAAAAAAAAAAAAAAAA-3' (cDNA1(n0))

(**9**) 5'-CCCTTTAACCCCAGACTCTTGAGTTCTCAGTATG-3' (pDNA2)

(**10**) 5'-CATACTGAGAACTCAAGAGTCT-3' (H5N1, tDNA2)

(**11**) 5'-A_{20}-CATACTGAGAACTCAA-3' (cDNA2(n16)).

Instruments. Fluorescence Hitachi F-4600 fluorescence spectrophotometer were performed to collect the fluorescence spectra data of RpDNA1/cDNA1(n)-Ag NCs, RpDNA1/cDNA1(n)-Ag NCs with different volume of GO solution, RpDNA1-Ag NCs, RpDNA1-Ag NCs/cDNA1(n)/GO nanocomposite in the absence and presence of target genes tDNA1, GpDNA2-Ag NCs, GpDNA2-Ag NCs/cDNA2(n)/GO nanocomposite in the absence and presence of tDNA2. The green-emitting ssDNA-Ag NCs were excited at λ_{ex} = 448 nm. The red-emitting ssDNA-Ag NCs were excited at λ_{ex} = 525 nm. Agilent Cary 5000 UV-vis-NIR spectrophotometer were performed to collect the optical absorbance determination data.

Synthesis of Fluorescent ssDNA Templated Silver Nanoclusters. The ssDNA templated silver nanoclusters (pDNA/cDNA(n)-Ag NCs) were synthesized according to our reported approaches with minor modification.[28,29] The equivalent amount of ssDNAs of DNA **1** (pDNA1) and DNA **3**−**7** (cDNA1(n)) were mixed fully with 20 mM citrate buffer (pH 7.0) and were heated at 95 °C for 10 min. The solution then was annealed quickly in the ice bath for 30 min. After that, a certain concentration of Ag NO_3 working solution was introduced with vigorous shaking for 2 min and was placed into the ice bath for another 10 min. Next, the freshly prepared $NaBH_4$ was added to the mixture solution with vigorous shaking for 5 min. The product solutions red-emitting RpDNA1/cDNA1(n)-Ag NCs were kept in darkness and stored at 4 °C for overnight before the assays. As the control assay, sole A_{20} without tethering any bases of tDNA1 is coded as DNA **8**. Moreover, red-emitting RpDNA1-Ag NCs and green-emitting GpDNA2-Ag NCs were prepared as follows, using DNA **1** (pDNA1) and DNA **9** (pDNA2) as the template.[27] Certain volume of $AgNO_3$ working solution was added and kept at 0 °C for 10 min. After that, the $NaBH_4$ solution was introduced into the mixture under vigorously shaking for another 5 min. The product solutions including red-emitting RpDNA1-Ag NCs and green-emitting GpDNA2-Ag NCs were kept in darkness and stored at 4 °C for overnight before the assays. The ratio of ssDNA template:Ag-NO_3:$NaBH_4$ is 1:6:6.

Quantum Yield Measurements. The quantum yield (QY) of prepared ssDNA-Ag NCs was determined by the comparative method. Sulforhodamine 101 in ethanol (QY = 0.95) was chosen as a standard for red-emitting RpDNA1/cDNA(16)-Ag NCs and RpDNA1-Ag NCs. Rhodamine 6G in in ethanol (QY = 0.95) was selected as a standard for green-emitting GpDNA2-Ag NCs. The quantum yields of RpDNA1/cDNA1(16)-Ag NCs, RpDNA1-Ag NCs, and GpDNA2-Ag NCs in water were calculated according to the following formula:[30]

$$\Phi = \Phi_R\left(\frac{F}{F_R}\right)\left(\frac{A_R}{A}\right)\left(\frac{\eta}{\eta_R}\right)^2$$

where Φ is the quantum yield, F the integrated emission intensities (areas) measured, A the absorbance at the excitation wavelength, and η the refractive index of the solvent. The subscript "R" refers to the reference standard with definite quantum yield. Moreover, the optical absorbance determination (A) was maintained below 0.1 to minimize the reabsorption effect.

Multiplexed Analysis of Target DNAs Using pDNA-Ag NCs/cDNA(n)/GO Probe Based on a Toehold-Mediated Strand Displacement Reaction Mechanism. In the typical DNA assay, the constructed pDNA-Ag NCs/cDNA(n)/GO nanohybrid materials were hybridized with varies of concentrations of target DNAs (DNA **2** and DNA **10**) in phosphate buffer (20 mM, pH 7.0) and incubated for 30 min. After that, fluorescence spectra were then measured.

RESULTS AND DISCUSSION

Principle of Target-Activated Multiplex Analysis Using Ag NCs/GO Nanohybrid Materials Based on a Toehold-Mediated Strand Displacement Strategy. In order to construct an activated fluorescent probe, ssDNA templated Ag NCs, one type of new promising fluorescent nanomaterials, are chosen as the energy donor, while GO is selected as the energy acceptor, because of its broad-spectrum fluorescent quenching characteristic. How does one develop the activatable probe based on a toehold-mediated strand displacement reaction for detaching Ag NCs from the GO surface? Inspired by the reported work,[31] fluorescent dye-labeled probe DNA (pDNA), capture DNA (cDNA), and target DNA (tDNA) are needed in the performed assays. As

https://doi.org/10.1021/acs.analchem.1c03570
Anal. Chem. 2021, 93, 16025−16034

the proof of concept, the biomarker Influenza A virus subtype gene H1N1 (tDNA1) is chosen as the target model for further experimental assays. In the typical assay, the red-emitting fluorescent silver nanoclusters tethering the complementary sequence of virus subtype gene H1N1 are designed and synthesized as the pDNA1 (RpDNA1-Ag NCs) (see Scheme S1 in the Supporting Information). The capture DNA (cDNA1) is a bifunctional single-stranded DNA fragment consisting of a partial sequence of target gene H1N1 (tDNA1) and poly adenine sequence (A_{20}) tail (Scheme S1). Since the partial sequence of cDNA1 can specifically capture the pDNA1 to form partially complementary double-stranded DNA (dsDNA) (pDNA1/cDNA1), the A_{20} sequence can anchor the cDNA1 to the surface of GO, because of its high affinity to the GO, achieving the aim of indirectly adsorbing pDNA1 on the GO matrix (Scheme S1, Route I). In the absence of tDNA1, cDNA1 specifically recognizes pDNA1 and forms the partially complementary double-stranded DNA structure (RpDNA1-Ag NCs/cDNA1). As for the high affinity of the A_{20} tail conjugating cDNA1 to GO, RpDNA1-Ag NCs/cDNA1 composites are immobilized on the surface of GO. It does not nearly display fluorescence signal for RpDNA1-Ag NCs/cDNA1/GO nanocomposites as for the energy transfer mechanism (Scheme S1, Route II). After that, a toehold-mediated strand displacement reaction is introduced for detaching pDNA1 (RpDNA1-Ag NCs) from the quencher GO surface. It is expected that the strand displacement reaction might lead to the formation of a stable pDNA1/tDNA1 duplex strands structure, resulting in the desorption of the pDNA1 from cDNA1/GO complex. Thus, it will turn up remarkable fluorescent enhancement phenomenon that can be attributed to disruption of the energy transfer process after the addition of tDNA1. However, to achieve this goal, two issues must be addressed.

First Issue: The Choice of the Synthesis Route for Preparing Fluorescent Ag NCs. The first issue is which synthesis route should be chosen for preparing fluorescent probe pDNA (Scheme 2, upper figure). One route is that pDNA1 first binds with the capture DNA (cDNA1) to form partially complementary double-stranded DNA structure, which is then selected as the template to synthesize red-emitting fluorescence silver nanoclusters in situ (Route I). Meanwhile, the other route is that pDNA1 is directly selected as the scaffold for preparing red-emitting fluorescent Ag NCs before binding with cDNA1 (Route II).

The one synthesized route is first performed (see Scheme 2). The bifunctional ssDNA fragment consisting of the scaffold sequence for synthesizing red-emitting Ag NCs and the complementary sequence fragment of target H1N1 gene sequence is designed and coded as DNA **1** (called pDNA1, Scheme S1). The target virus subtype gene H1N1 sequence is coded as DNA **2** (named tDNA1). In order to initiate the toehold-mediated strand displacement reaction, capture ssDNA (called cDNA1) is also designed, which consists of the partial fragment of tDNA1 and poly adenine (A_{20}) sequence (Scheme S1). Considering sticky ends generally consist of 6−10 bases for efficiently initiating the toehold-mediated strand displacement reaction,[32] varying base lengths of the complementary fragment between pDNA1 and cDNA1 including *n*16, *n*14, *n*12, *n*10, and *n*8 are designed and implemented for the further assays (see Scheme 2, as well as Scheme S1). The capture cDNA1(*n*16) including 16 bases length of tDNA1 tethering A_{20} tail is coded as DNA **3**. Similarly, cDNA1(*n*14), cDNA1(*n*12), cDNA1(*n*10), and cDNA1(*n*8), possessing 14, 12, 10, and 8 bases length of tDNA1 conjugating an A_{20} tail, are coded as DNA **4**, **5**, **6**, and **7**, respectively. Meanwhile, sole A_{20} without tethering any bases of tDNA1 is called DNA **8**, which is used as the comparative assay.

In a typical protocol, equimolar pDNA1 and cDNA1(*n*16) are mixed thoroughly and then subjected to annealing treatment to form the partial complementary double-stranded DNA fragment (called pDNA1/cDNA1(*n*16) structure). After that, pDNA1/cDNA1(*n*16) fragment is chosen as the template for synthesizing red-emitting fluorescent Ag NCs in situ, which are called RpDNA1/cDNA1(*n*16)-Ag NCs, according to our reported method with little modification.[33] Via a similar synthesis route, red-emitting RpDNA1/cDNA1(*n*14)-Ag NCs, RpDNA1/cDNA1(*n*12)-Ag NCs, RpDNA1/cDNA1(*n*10)-Ag NCs, and RpDNA1/cDNA1(*n*8)-Ag NCs are also prepared (Scheme 2, route I). In order to further investigate the detailed change of fluorescent signal of preprepared Ag NCs, pDNA1 without binding with cDNA1 fragment is also applied for synthesizing red-emitting RpDNA1/cDNA1(*n*0)-Ag NCs, based on the same synthesized process described above. Surprisingly, the unexpected results are indicated in Figure S1 in the Supporting Information. The maximum emission intensity of prepared Ag NCs changes with the varying complementary base length of cDNA1. The differentiation of fluorescent emission intensity can be clearly observed from Figure S2 in the Supporting Information. The experimental results reveal the number of complementary base pairs (*n*) in a partial-complementary duplex-strands pDNA1/cDNA1 structure can affect the fluorescence of the synthesized Ag NCs as follows: *n*16 > *n*0 > *n*14 > *n*10 > *n*12 > *n*8, to some extent. Besides, the detailed fluorescence spectral parameters and the order of emission intensity are listed in Table S1 in the Supporting Information. As displayed in Figure S3 in the Supporting Information, only the cDNA1(*n*16) fragment induces the remarkable fluorescence enhancement of synthesized Ag NCs, in comparison to the standard (the maximum emission intensity of RpDNA1/cDNA1(*n*0)-Ag NCs). In contrast, other capture DNAs including cDNA1(*n*14), cDNA1(*n*12), cDNA1(*n*10), and cDNA1(*n*8) only lead to decreased fluorescent signal of Ag NCs. We guess that the capture DNA1, as a partial sequence of H1N1, own the function of inducing remarkable fluorescent enhancement of Ag NCs, which is similar to the reported guanine-proximity-induced fluorescence enhancement mechanism.[34,35] The cDNA1(*n*16), consisting of 16 bases length of target H1N1 tethering A_{20} tail, possesses the longest similar sequence of H1N1 sequence among all capture cDNA1s (*n* = 16, 14, 12, 10, 8), then resulting in the most significant fluorescence enhancement of Ag NCs.

After that, the other synthesis route is also performed. The sole DNA **1** is selected as the scaffold to directly fabricate fluorescent Ag NCs. Then, the capture DNAs are introduced and incubated for 30 min at room temperature via vortex approach to form RpDNA1-Ag NCs/cDNA1 nanocomposite with partial complementary dsDNA fragment (Scheme 2, Route II). Figure S4 suggests that even binding with the cDNA1(*n*16) fragment only induces a slightly decreased fluorescence intensity of the prepared pDNA1-Ag NCs, revealing that the addition sequence of cDNA1(*n*16) plays an important role in the fluorescence enhancement of pDNA-Ag NCs. In other words, after the synthesis of fluorescent Ag

https://doi.org/10.1021/acs.analchem.1c03570
Anal. Chem. 2021, 93, 16025−16034

NCs, cDNA1(*n*16) binding behavior does not distinguishably enhance the fluorescence signal of RpDNA1-Ag NCs. Meanwhile, other cDNA1(*n*14), cDNA1(*n*12), cDNA1(*n*10), and cDNA1(*n*8) binding process also do not induce significant change of RpDNA1-Ag NCs (Figure S5 in the Supporting Information). However, which synthesis route should be chosen for the further assay cannot still be decided so far.

Second Issue: The Activated Behavior of the Quenching Ag NCs/GO Composites by Adding Analytes Based on Toehold-Mediated Strand Displacement Reaction. The second issue is whether or not activated fluorescent enhancement can be achieved, based on a toehold-mediated strand displacement reaction (Scheme S1, lower figure). It should be divided into two steps with two small problems. The first problem involves how the quenching efficiency of GO for the prepared fluorescent Ag NCs is determined. The second problem is whether or not the fluorescent activation can be realized after adding the target. To address these two small problems, preprepared Ag NCs by using two synthesized routes are selected for the further assays.

Among the fluorescent Ag NCs synthesized via the first route, RpDNA1/cDNA1(*n*16)-Ag NCs possess the highest fluorescence intensity and are chosen for the further study model for the fluorescence quenching and activation probe construction assays. The response of fluorescent emission spectra of RpDNA1/cDNA1(*n*16)-Ag NCs in the absence and presence of varies concentrations of GO is performed and the results are displayed in Figure S6 in the Supporting Information. The fluorescence spectrum of RpDNA1/cDNA1-(*n*16)-Ag NCs without adding GO exhibits strong fluorescent emission signal. However, after the introduction of quencher GO, it appears significant decrease of red-emitting fluorescent Ag NCs. The quenching rate of the emission signal is calculated (up to 76.8%) (Figure S6, curve 10). The experimental situations indicate strong adsorption of A_{20} tail tethering the RpDNA1/cDNA1(*n*16)-Ag NCs on GO surface and high fluorescent quenching efficiency of GO. As for the high affinity of A_{20} tail to GO, RpDNA1/cDNA1(*n*16)-Ag NCs nanocomposite indirectly adsorbs to the surface of GO. After that, because of the occurrence of energy transfer behavior from donor Ag NCs to acceptor GO (Scheme S1), it appears as a significant fluorescent quenching phenomenon. In addition, the activation assay of RpDNA1/cDNA1(*n*16)-Ag NCs/GO complex with incubating with target DNA **2** is then performed. However, it does not still turn up the remarkable enhancement of quenching fluorescence signal of RpDNA1/cDNA1(*n*16)-Ag NCs/GO nanocomposites, even after the introduction of high concentration of tDNA1 with 20 μM (see Figure S7 in the Supporting Information). Thus, our construction strategy still needs to be further adjusted.

Then, red-emitting fluorescent RpDNA1-Ag NCs by the second route are synthesized and then incubated with cDNA1(*n*16) for forming RpDNA1-Ag NCs/cDNA1(16) nanocomplex attributing to the formation of partially complementary duplex strands DNA structure (Scheme 2, Route II). The assay results reveal that the addition of cDNA1(*n*16) does not remarkably change the fluorescence intensity of RpDNA1-Ag NCs in this approach (see Figure S8, curves 1 and 2, in the Supporting Information. However, upon the introduction of fluorescent quencher GO, the RpDNA1-Ag NCs/cDNA1(*n*16) composites absorb on the GO surface via the high affinity of A_{20} tail, resulting in the quenching fluorescence of RpDNA1-Ag NCs/cDNA1(*n*16)/GO complex (see Figure S8, curve 3) because of the energy transfer process from the donor RpDNA1-Ag NCs/cDNA1(*n*16) to acceptor GO (Scheme S1, Route II). The next step is to implement the activation fluorescent assay. Figure 1A depicts the fluorescence

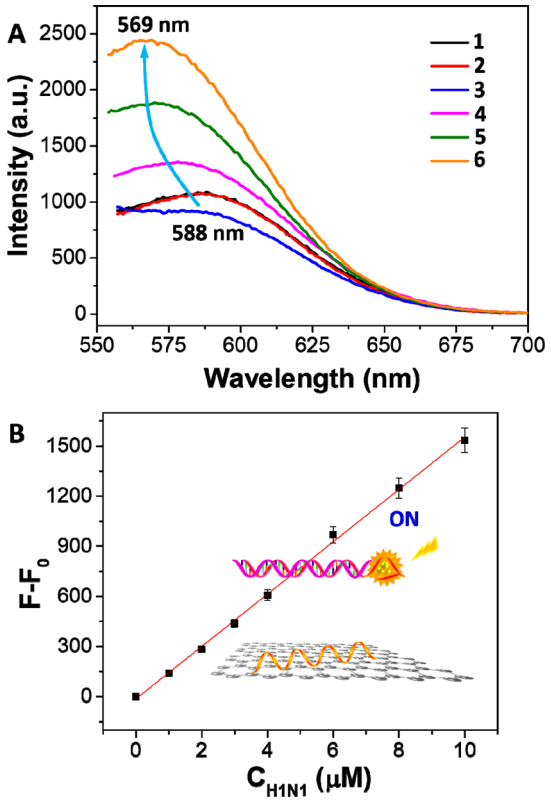

Figure 1. (A) Fluorescence spectra of RpDNA1-Ag NCs/cDNA1-(*n*16)/GO complex in the presence of different amounts of DNA **2** from 0 to 10 μM. Conditions: 1, RpDNA1-Ag NCs; 2, RpDNA1-Ag NCs/cDNA1(*n*16); 3, RpDNA1-Ag NCs/cDNA1(*n*16)/GO complex; 4–6: 3 + DNA **2** (μM): 3, 6, and 10. (B) The linear correlation between fluorescence intensity increments ($F-F_0$) of the RpDNA1-Ag NCs/cDNA1(*n*16)/GO composite versus the concentrations of DNA **2** from 0 to 10 μM.

spectra of the desorbed Ag NCs from the GO matrix upon incubating with different concentrations of target DNA **2** (tDNA1, H1N1)-based on the target-induced desorption mechanism. DNA **2**, as a model, efficiently initiates the operation of a toehold-mediated strand displacement reaction, forming complete-complementary duplex-stranded DNA structure (RpDNA1-Ag NCs/tDNA1), leading to the detachment behavior of RpDNA1-Ag NCs from GO surface, and leading to enhanced fluorescence (Scheme S1, Route II). As the concentration of the DNA **2** increases, the resulting activatable fluorescence signal is gradually intensified. Control experiments revealed that the introduction of DNA **2** does not result in significant changes in the fluorescence intensity of the Ag NCs in the absence of GO. Figure 1B illustrates the linear correlation between the increment of fluorescent intensity ($F-F_0$) of RpDNA1-Ag NCs/cDNA1(*n*16)/GO nanocomposite versus varies of the concentrations of the target DNA **2**. By analyzing the change of fluorescence of the sensor after adding the concentrations of DNA **2**, a linear relationship between the fluorescence increment and the concentrations of DNA **2** over a range of 0.002 μM to 10 μM is obtained. The detection limit of H1N1 is calculated as 0.1 nM.

https://doi.org/10.1021/acs.analchem.1c03570
Anal. Chem. 2021, 93, 16025−16034

Besides, it is clearly observed that the quenching fluorescence signal of RpDNA1-Ag NCs/cDNA1(*n*16)/GO nanocomposite increases gradually with the increasing concentrations of DNA **2** (Figure 2A). The high recovery

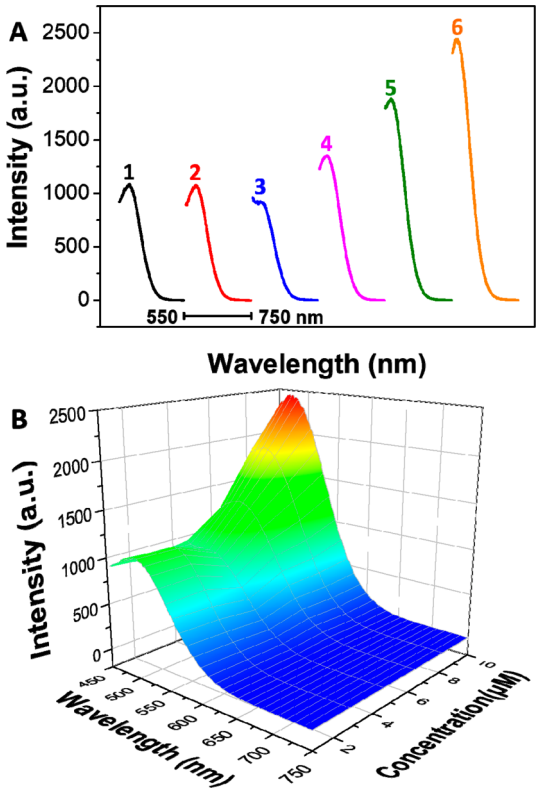

Figure 2. (A) Fluorescence emission spectra of RpDNA1-Ag NCs/cDNA1(*n*16)/GO nanocomposites upon the addition of different concentrations of target DNA **2**. (B) Three dimensional fluorescence spectrum of RpDNA1-Ag NCs/cDNA1(*n*16)/GO nanocomposites after the addition of different concentrations of DNA **2**. Conditions: 1, RpDNA1-Ag NCs; 2, RpDNA1-Ag NCs/cDNA1(*n*16); 3, RpDNA1-Ag NCs/cDNA1(*n*16)/GO; 4−6:3 + DNA **2** (μM): 3, 6, and 10.

rate with 823.35% is obtained by using the increment of fluorescence signal of the sensor after adding 10 μM H1N1 divided by the decrement of fluorescent intensity of RpDNA1-Ag NCs/cDNA1(*n*16) in the presence of 25 μg/mL quencher GO (see Figure S9 in the Supporting Information). Moreover, a three-dimensional (3D) fluorescence pattern is made to further show distinct changes with the gradually increasing concentrations of DNA **2** (Figure 2B).

In addition, to further explore the differentiation of fluorescent signal of RpDNA1-Ag NCs/cDNA1(*n*16) composite before the adsorption to GO and after the desorption from the GO surface, the differentiating emission curves and CIE1931 chromaticity coordinate calculation image are also conducted (Figure 3). The fluorescent emission spectra of preprepared RpDNA1-Ag NCs/cDNA1(*n*16) composite, RpDNA1-Ag NCs/cDNA1(*n*16) in the presence of 25 μg/mL GO, and RpDNA1-Ag NCs/cDNA1(*n*16)/GO complex after the addition of 10 μM DNA **2** are shown in Figure 3A. Interestingly, it appears a remarkable blue-shift from 588 nm to 569 nm of maximum emission peak of RpDNA1-Ag NCs/cDNA1(*n*16)/GO complex after the addition of DNA **2** (Figure 3A). Figure 3B displays the significant differentiation

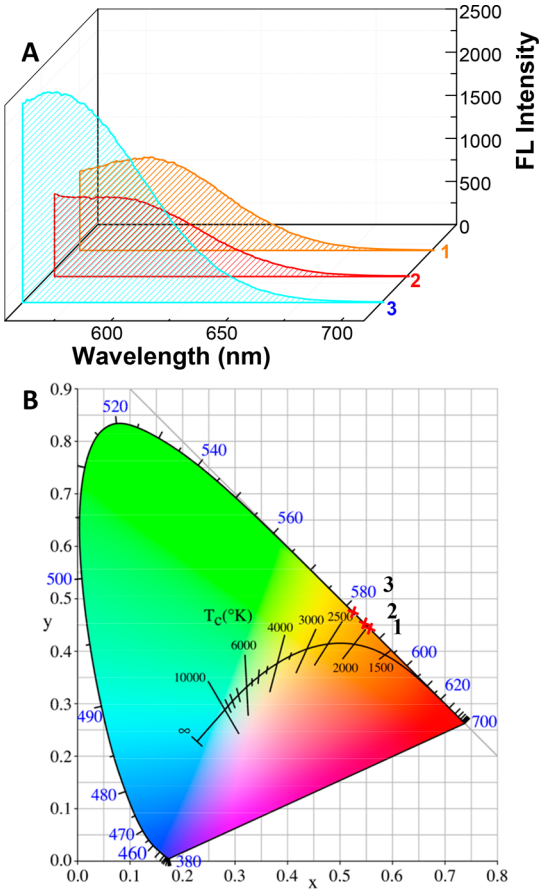

Figure 3. (A) Differentiating fluorescent emission characteristics and (B) image of the CIE1931 chromaticity coordinate calculation of preprepared RpDNA1-Ag NCs/cDNA1(*n*16) (1), RpDNA1-Ag NCs/cDNA1(*n*16) in the presence of 25 μg/mL GO (2), RpDNA1-Ag NCs/cDNA1(*n*16)/GO incubating with 10 μM DNA **2** (3).

of emission color change of RpDNA1-Ag NCs/cDNA1(*n*16) before the adsorption and after the desorption from the GO surface. Therefore, based on the toehold-mediated strand displacement mechanism, a novel activatable platform for sensing virus subtype gene H1N1, by using DNA-templated Ag NCs/GO nanohybrid material, has been proposed.

Similarly, the green-emitting fluorescent Ag NCs are synthesized by using DNA **9** (pDNA2) as the template, named as GpDNA2-Ag NCs. Virus subtype gene H5N1 sequence is chosen as the model, named as target DNA **10** (tDNA2). As shown in Figure 4A, synthesized GpDNA2-Ag NCs exhibit quite a strong fluorescence signal with the maximum emission located at 530 nm (curve 1, Figure 4A). Then, the addition of capture DNA **11** (named cDNA2(*n*16)) leads to the certain decrease of fluorescence signal of GpDNA2-Ag NCs, because of the formation of GpDNA2-Ag NCs/cDNA2(*n*16) complex due to partially complementary duplex-strands conformation (curve 2), disturbing the microenvironment of fluorescent Ag NCs. After that, it appears the remarkable fluorescence quenching of GpDNA2-Ag NCs/cDNA2(*n*16) complex after the introduction of quencher GO attributing to the adsorption of GpDNA2-Ag NCs/cDNA2-(*n*16) composite to the GO surface and the occurrence of energy transfer from donor GpDNA2-Ag NCs/cDNA2(*n*16) to acceptor GO (curve 3). Interestingly, upon the addition of

https://doi.org/10.1021/acs.analchem.1c03570
Anal. Chem. 2021, 93, 16025−16034

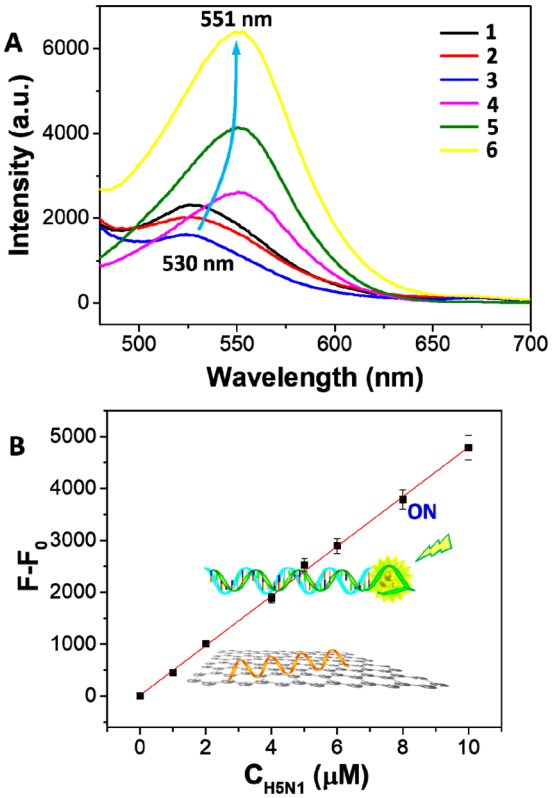

Figure 4. (A) The fluorescence spectra of GpDNA2-Ag NCs/cDNA2(n16)/GO complex in the presence of different amounts of DNA **10** from 0 to 10 μM. Conditions: 1, GpDNA2-Ag NCs; 2, GpDNA2-Ag NCs/cDNA2(n16); 3, GpDNA2-Ag NCs/cDNA2-(n16)/GO composite; 4−6:3 + DNA **10** (μM): 2, 5, and 10. (B) The linear correlation between fluorescence intensity change ($F-F_0$) of the GpDNA2-Ag NCs/cDNA2(n16)/GO composite versus the concentration of DNA **10** from 0 to 10 μM.

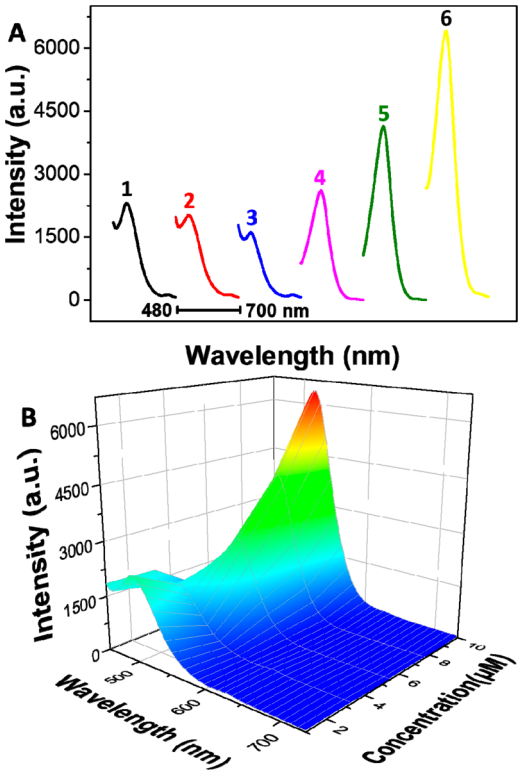

Figure 5. (A) Fluorescence emission spectra of GpDNA2-Ag NCs/cDNA2(n16)/GO nanocomposites upon the addition of different concentrations of target DNA **10**. (B) Three-dimensional fluorescence spectrum of GpDNA2-Ag NCs/cDNA2(n16)/GO nanocomposites upon the addition of different concentrations of target DNA **10**. [Conditions: 1, GpDNA2-Ag NCs; 2, GpDNA2-Ag NCs/cDNA2(n16); 3, GpDNA2-Ag NCs/cDNA2(n16)/GO complex; 4−6:3 + DNA **10** (μM): 2, 5, and 10.]

DNA **10**, significant enhancement is observed (curve 4) with a remarkable red-shift emission peak located at 551 nm. As the concentration of DNA **10** increases, the resulting fluorescence is gradually intensified (curve 5 and 6, Figure 4A). This may be due to the process of the formation of the GpDNA2-Ag NCs/tDNA2 fully complementary double-stranded DNA structure based on a toehold-mediated strand displacement reaction, leading to the desorption of GpDNA2-Ag NCs from the GO surface and activating the fluorescence signal. Moreover, a linear range from 0.1 nM to 10000 nM and a detection limit of 0.01 nM for target DNA **10** detection are obtained (Figure 4B).

Besides, the detailed fluorescence change of GpDNA2-Ag NCs/cDNA2(n16) nanocomposites before the adsorption and after the desorption of GO is displayed in Figure 5A. The fluorescent recovery rate is calculated (693.62%) by using the increment of fluorescence signal after adding 10 μM DNA **10** divided by the decrement of fluorescent intensity of GpDNA2-Ag NCs/cDNA2(n16) with 25 μg/mL quencher GO (see Figure S10 in the Supporting Information). The fluorescence signal gradually increases with the rising concentrations of DNA **10** from Figure 5A, which is consistent with the results obtained from the 3D fluorescence spectrum (Figure 5B).

In addition, in order to further differentiate the color and intensity variation, different emission characteristic curves and CIE1931 chromaticity coordinate calculation are also performed (Figure 6). The differentiating fluorescent emission characteristics of prepared GpDNA2-Ag NCs/cDNA2(n16), GpDNA2-Ag NCs/cDNA2(n16) in the presence of 25 μg/mL quencher GO, and GpDNA2-Ag NCs/cDNA2(n16)/GO composites with 10 μM DNA **10** are displayed in Figure 6A. The more clear change of emission wavelength and intensity can be observed based on a toehold-mediated strand displacement reaction. Meanwhile, the subtle difference can be seen more intuitively from the CIE1931 chromaticity coordinate calculation image (Figure 6B). Thus, a new approach for the detection of virus subtype gene H5N1 is first developed based on a toehold-mediated strand displacement mechanism by using GpDNA2-Ag NCs/cDNA2(n16)/GO nanocomposite.

Through a series of above experimental exploration and research, a new approach for activatable fluorescent sensor based on ssDNA-Ag NCs/GO hybrid nanocomposites by using a toehold-mediated strand displacement reaction mechanism is successfully constructed and applied in the detection of virus genes. Besides, the stability of our proposed method is also performed. It suggests that the fluorescence intensity of synthesized RpDNA1-Ag NCs and RpDNA1-Ag NCs/cDNA1(n16)/GO incubated with 10 μM target DNA **2** remained almost unchanged within 1 month (a <10% decrease in the emission intensities), revealing good stability (see Figure S11 in the Supporting Information).

Multichannel Analysis of Genes Simultaneously. A multiplexed fluorescent approach provides more improvement in the accurate diagnosis of clinical disease than single gene

https://doi.org/10.1021/acs.analchem.1c03570
Anal. Chem. 2021, 93, 16025−16034

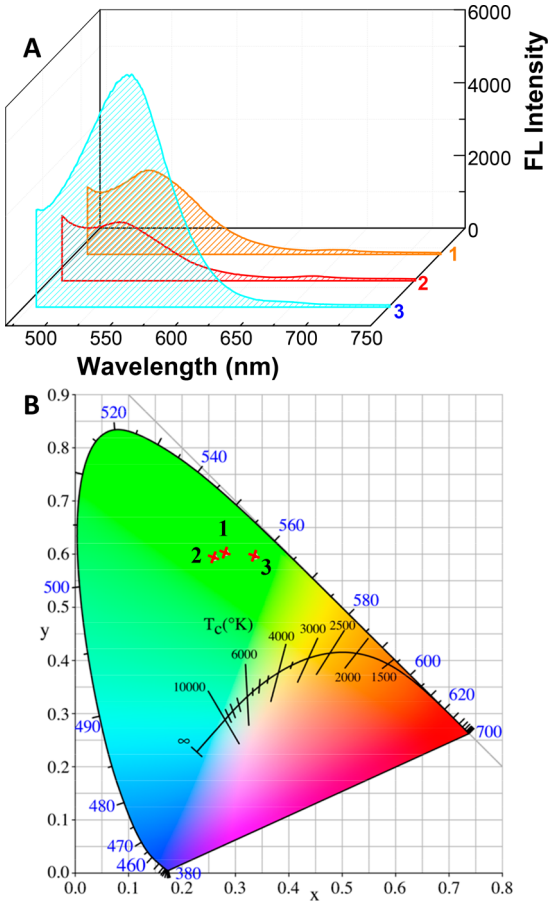

Figure 6. (A) Differentiating fluorescent emission characteristics and (B) image of the CIE1931 chromaticity coordinate calculation of preprepared GpDNA2-Ag NCs/cDNA2($n16$) (1), GpDNA2-Ag NCs/cDNA2($n16$) + 25 μg/mL GO (2), GpDNA2-Ag NCs/cDNA2($n16$)/GO composites +10 μM DNA **10** (3).

analysis, thereby attracting more widespread interest among scientists in different fields.[36−38] However, it is still challenging research for developing multiplexed methods, because of the need of multiple labeling of different reporters and mutual interference among different signal units.[28,33,39,40] Our experimental assay results suggest that our proposed approach can be applied for the multichannel detection of two types of virus subtype genes (Scheme 3). The introduction of H1N1 and H5N1 can significantly activate the quenched fluorescence of RpDNA1-Ag NCs/cDNA1($n16$) and GpDNA2-Ag NCs/cDNA2($n16$) /GO complex, while the coexistence signal reporter units do not interfere each other, displaying their promising application for multiple targets in real samples (Figure S12 in the Supporting Information). More interesting, the activation process efficiently modulates the emission wavelength of silver nanoclusters with a green-emitting GpDNA2-Ag NCs emission bathochromic shift (21 nm) and a red-emitting RpDNA1-Ag NCs emission hypsochromic shift (19 nm), compared with the fluorescence of Ag NCs before activation, which is called a chemopalette. Thus, the novel multiple analysis of genes is proposed with the assistance of toehold displacement and Ag NCs/GO nanohybrid materials.

Further Investigation of Enhancement and Wavelength Shift of a Ag NCs/GO Complex Undergoing a Configuration Transformation. Our previous research demonstrates that H1N1 fragment proximity plays an important role in the fluorescence enhancement,[33] which is similar to the guanine-rich DNA proximity.[41,42] In this study, only the addition of cDNA1($n16$) to RpDNA1 before the synthesis of fluorescence Ag NCs can trigger the distinguishable enhancement while the addition of cDNA1($n16$) after the preparation of fluorescence Ag NCs nearly does not induce enhanced fluorescence. As cDNA1(16) consists of 16 bases length of H1N1 tethering A_{20} tail which possesses more similar base number as H1N1 than other cDNA1($n14$, 12, 10, 8), RpDNA1/cDNA1($n16$)-Ag NCs display the maximum fluorescence intensity (see Figure S2 in the Supporting Information). Thus, we guess that H1N1 proximity is beneficial for different fluorescence properties of Ag NCs synthesized by two types of synthetic routes.

In order to obtain a deeper understanding of the origin of the enhancement effect of fluorescent Ag NCs in our proposed approach, the fluorescent quantum yield (QY) determination assays were performed. The QY of RpDNA1-Ag NCs, RpDNA1-Ag NCs/cDNA1($n16$), and RpDNA1-Ag NCs/cDNA1($n16$)/GO complex incubating with 10 μM H1N1 were calculated as 7.5%, 7.4%, and 16.8%, respectively, by using sulforhodamine 101 (QY = 95%) as a standard (Table S2 in the Supporting Information). Meanwhile, the QY of GpDNA2-Ag NCs, GpDNA2/cDNA2 ($n16$)-Ag NCs, GpDNA2/cDNA2($n16$)-Ag NCs/GO composite incubating with 10 μM H5N1 were determined to be 16.0%, 13.7%, and 35.8%, respectively, by using Rhodamine 6G (QY = 95%) as a standard (see Table S2). These experimental results reveal that the quantum yield of silver nanoclusters can be efficiently improved in our present construction strategy, even accompanying tunable emission wavelength shift, providing a new avenue for modulating the fluorescent intensity and emission wavelength of DNA-templated silver nanoclusters.

Scheme 3. Schematic Representation of Multichannel Analysis of Genes Simultaneously of Indirect Adsorption Chemopalette ssDNA-Ag NCs/GO Nanohybrid Materials Based on a Toehold-Mediated Strand Displacement Reaction Mechanism[a]

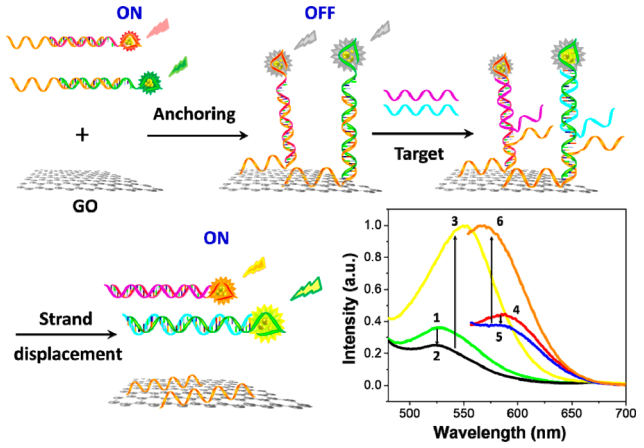

[a]The inserted figure is the bathochromic shift emission curves of GpDNA2-Ag NCs/cDNA2($n16$)/GO composites and the hypsochromic shift emission curves of RpDNA1-Ag NCs/cDNA1($n16$)/GO composites.

CONCLUSIONS

In summary, the ssDNA-Ag NCs/GO hybrid materials system has been successfully applied in the construction of an

https://doi.org/10.1021/acs.analchem.1c03570
Anal. Chem. 2021, 93, 16025−16034

activatable sensing platform for multiple genes detection. This strategy adopts GO as the quencher and vehicle while fluorescence Ag NCs as the donor with the assistance of a toehold-mediated strand displacement mechanism, which brings about unique indirect DNA adsorption method for constructing DNA/GO-hybrid-material-based versatile platform, helping enhance the signal contrast for the target detection and improve emission recovery and sensitivity. More interestingly, the detachment behavior of pDNA-Ag NCs from the GO surface effectively modulates the emission wavelength and intensity of Ag NCs, providing a novel way for obtaining tuning fluorescence Ag NCs which is totally different from traditional methods through by changing DNA template bases or conformation. Our present study enriches the preparation methods of fluorescence Ag NCs, which also effectively expend the application of Ag NCs. Moreover, the developed toehold displacement Ag NCs/GO biosensor is applied for multichannel sensitive detection of subtype virus genes H1N1 and H5N1 successfully. The experimental results suggest that our present approach exhibits much higher or comparable sensitivity than the fluorescence methods reported (see Table S3 in the Supporting Information).[28,33,43−48] Furthermore, the proposed strategy can be extended to other genes detection and possess a promising application in the field of clinical precision diagnosis and treatment.

■ ASSOCIATED CONTENT

Supporting Information

The Supporting Information is available free of charge at https://pubs.acs.org/doi/10.1021/acs.analchem.1c03570.

Schematic representation of how to construct an activatable fluorescent sensor of indirect adsorption chemopalette ssDNA-Ag NCs/GO nanohybrid materials; fluorescence excitation and emission spectra; detailed fluorescence spectral parameters of synthesized RpDNA1/cDNA1(n)-Ag NCs; change curves of emission intensity; histogram of emission intensity of preprepared RpDNA1-Ag NCs; effects of GO concentration on the fluorescence responses of the synthesized RpDNA1/cDNA1(n16)-Ag NCs; emission curve of the RpDNA1/cDNA1(n16)-Ag NCs/GO nanocomposites; investigation on the stability of fluorescent silver nanoclusters; fluorescence quantum yield of synthesized RpDNA1-Ag NCs, RpDNA1-Ag NCs/cDNA1(n16), and RpDNA1-Ag NCs/cDNA1(n16)/GO; summary of the reported fluorescence DNA sensing methods (PDF)

■ AUTHOR INFORMATION

Corresponding Author

Guoliang Liu − *School of Chemistry and Chemical Engineering, Yancheng Institute of Technology, Yancheng 224051, China;* orcid.org/0000-0002-2969-1816; Phone: +86-515-88298190; Email: liuguoliang199@126.com, glliu@ycit.edu.cn

Author

Da-Qian Feng − *School of Chemistry and Chemical Engineering, Yancheng Institute of Technology, Yancheng 224051, China;* orcid.org/0000-0002-9351-3918

Complete contact information is available at: https://pubs.acs.org/10.1021/acs.analchem.1c03570

Notes

The authors declare no competing financial interest.

■ ACKNOWLEDGMENTS

This work is sponsored by the National Natural Science Foundation of China (No. 21501146), and the Natural Science Foundation of Jiangsu Province (Nos. BK20150424 and BK20140464), the Opening Foundation of the Key Laboratory for Preparation and Application of Ordered Structural Materials of Guangdong Province (No. KLPAOSM201507), the Opening Project of Jiangsu Key Laboratory of Biochemistry and Biotechnology of Marine Wetland (No. K2016-18), and the Qinglan Project of Jiangsu Province and Jiangsu Overseas Visiting Scholar Program for University Prominent Young and Middle-aged Teachers and Presidents.

■ REFERENCES

(1) Li, J. J.; Cheng, F. F.; Huang, H. P.; Li, L. L.; Zhu, J. J. *Chem. Soc. Rev.* **2015**, *44*, 7855−7880.
(2) Medintz, I. L.; Clapp, A. R.; Brunel, F. M.; Tiefenbrunn, T.; Uyeda, H. T.; Chang, E. L.; Deschamps, J. R.; Dawson, P. E.; Mattoussi, H. *Nat. Mater.* **2006**, *5*, 581−589.
(3) Kobayashi, H.; Choyke, P. L. *Acc. Chem. Res.* **2011**, *44*, 83−90.
(4) Lee, S.; Xie, J.; Chen, X. Y. *Curr. Top. Med. Chem.* **2010**, *10*, 1135−1144.
(5) Kobayashi, H.; Ogawa, M.; Alford, R.; Choyke, P. L.; Urano, Y. *Chem. Rev.* **2010**, *110*, 2620−2640.
(6) Lyu, Y.; Pu, K. Y. *Adv. Sci.* **2017**, *4*, 1600481.
(7) Bremer, C.; Tung, C. H.; Weissleder, R. *Nat. Med.* **2001**, *7*, 743−748.
(8) Weissleder, R.; Tung, C. H.; Mahmood, U.; Bogdanov, A. *Nat. Biotechnol.* **1999**, *17*, 375−378.
(9) Yin, Y. M.; Chen, G. F.; Gong, L.; Ge, K. Z.; Pan, W. Z.; Li, N.; Machuki, J. O.; Yu, Y. Y.; Geng, D. Q.; Dong, H. F.; Gao, F. L. *Anal. Chem.* **2020**, *92*, 9247−9256.
(10) Li, N.; Shen, F. Z.; Cai, Z. H.; Pan, W. Z.; Yin, Y. M.; Deng, X.; Zhang, X.; Machuki, J. O.; Yu, Y. Y.; Yang, D. Z.; Yang, Y.; Guan, M.; Gao, F. L. *Small* **2020**, *16*, 2005511.
(11) Shi, Y. P.; Pan, Y.; Zhang, H.; Zhang, Z. M.; Li, M. J.; Yi, C. Q.; Yang, M. S. *Biosens. Bioelectron.* **2014**, *56*, 39−45.
(12) Zhao, Z. L.; Fan, H. H.; Zhou, G. F.; Bai, H. R.; Liang, H.; Wang, R. W.; Zhang, X. B.; Tan, W. H. *J. Am. Chem. Soc.* **2014**, *136*, 11220−11223.
(13) Wang, H. S.; Liu, H. L.; Wang, K.; Ding, Y.; Xu, J. J.; Xia, X. H.; Chen, H. Y. *Anal. Chem.* **2017**, *89*, 11366−11371.
(14) Satishkumar, B. C.; Brown, L. O.; Gao, Y.; Wang, C. C.; Wang, H. L.; Doorn, S. K. *Nat. Nanotechnol.* **2007**, *2*, 560−564.
(15) Morales-Narvaez, E.; Merkoci, A. *Adv. Mater.* **2012**, *24*, 3298−3308.
(16) Lu, C.-H.; Yang, H.-H.; Zhu, C.-L.; Chen, X.; Chen, G.-N. *Angew. Chem.* **2009**, *121*, 4879−4881.
(17) Chang, H.; Tang, L. H.; Wang, Y.; Jiang, J. H.; Li, J. H. *Anal. Chem.* **2010**, *82*, 2341−2346.
(18) Wang, Y.; Li, Z. H.; Hu, D. H.; Lin, C. T.; Li, J. H.; Lin, Y. H. *J. Am. Chem. Soc.* **2010**, *132*, 9274−9276.
(19) Huard, D. J. E.; Demissie, A.; Kim, D.; Lewis, D.; Dickson, R. M.; Petty, J. T.; Lieberman, R. L. *J. Am. Chem. Soc.* **2019**, *141*, 11465−11470.
(20) Tao, Y.; Li, M. Q.; Ren, J. S.; Qu, X. G. *Chem. Soc. Rev.* **2015**, *44*, 8636−8663.
(21) Guo, Y. H.; Pan, X. Y.; Zhang, W. Y.; Hu, Z. G.; Wong, K.-W.; He, Z. K.; Li, H.-W. *Biosens. Bioelectron.* **2020**, *150*, 111926.
(22) Simmel, F. C.; Yurke, B.; Singh, H. R. *Chem. Rev.* **2019**, *119*, 6326−6369.
(23) Chen, X.; Liu, N.; Liu, L. Q.; Chen, W.; Chen, N.; Lin, M.; Xu, J. J.; Zhou, X.; Wang, H. B.; Zhao, M. P.; Xiao, X. J. *Nat. Commun.* **2019**, *10*, 4675.

(24) Qian, L. L.; Winfree, E.; Bruck, J. *Nature* **2011**, *475*, 368−372.
(25) Zhu, J. B.; Zhang, L. B.; Li, T.; Dong, S. J.; Wang, E. K. *Adv. Mater.* **2013**, *25*, 2440−2444.
(26) You, M. X.; Zhu, G. Z.; Chen, T.; Donovan, M. J.; Tan, W. H. *J. Am. Chem. Soc.* **2015**, *137*, 667−674.
(27) Li, L. J.; Zhang, W. K.; Tang, X. F.; Li, Z. J.; Wu, Y. Z.; Xiao, X. J. *Chem. Commun.* **2020**, *56*, 8794−8797.
(28) Liu, G. L.; Li, J. J.; Feng, D.-Q.; Zhu, J. J.; Wang, W. *Anal. Chem.* **2017**, *89*, 1002−1008.
(29) Liu, G. L.; Feng, D. Q.; Mu, X. Y.; Zheng, W. J.; Chen, T. F.; Qi, L.; Li, D. *J. Mater. Chem. B* **2013**, *1*, 2128−2131.
(30) Grabolle, M.; Spieles, M.; Lesnyak, V.; Gaponik, N.; Eychmüller, A.; Resch-Genger, U. *Anal. Chem.* **2009**, *81*, 6285−6294.
(31) Xiao, X.; Li, Y. F.; Huang, C. Z.; Zhen, S. J. *Chem. Commun.* **2015**, *51*, 16080−16083.
(32) Yurke, B.; Turberfield, A. J.; Mills, A. P.; Simmel, F. C.; Neumann, J. L. *Nature* **2000**, *406*, 605−608.
(33) Feng, D.-Q.; Liu, G. L. *Anal. Chem.* **2021**, *93*, 8326−8335.
(34) Yeh, H.-C.; Sharma, J.; Shih, I.-M.; Vu, D. M.; Martinez, J. S.; Werner, J. H. *J. Am. Chem. Soc.* **2012**, *134*, 11550−11558.
(35) Chen, Y. A.; Vu, H. T.; Liu, Y. L.; Chen, Y. I.; Nguyen, T. D.; Kuo, Y. A.; Hong, S.; Chen, Y. A.; Carnahan, S.; Petty, J. T.; Yeh, H. C. *Chem. Commun.* **2019**, *55*, 462−465.
(36) Huang, Q. L.; Chen, B.; Shen, J. L.; Liu, L.; Li, J. J.; Shi, J. Y.; Li, Q.; Zuo, X. L.; Wang, L. H.; Fan, C. H.; Li, J. *J. Am. Chem. Soc.* **2021**, *143*, 10735−10742.
(37) Li, H. Y.; Lin, H. Y.; Lv, W. X.; Gai, P. P.; Li, F. *Biosens. Bioelectron.* **2020**, *165*, 112336.
(38) Zhang, J. P.; Li, C.; Zhi, X.; Ramon, G. A.; Liu, Y. L.; Zhang, C. L.; Pan, F.; Cui, D. X. *Anal. Chem.* **2016**, *88*, 1294−1302.
(39) Chang, J. F.; Wang, X.; Wang, J.; Li, H. Y.; Li, F. *Anal. Chem.* **2019**, *91*, 3604−3610.
(40) Zhou, W. J.; Zhu, J. B.; Fan, D. Q.; Teng, Y.; Zhu, X. Q.; Dong, S. J. *Adv. Funct. Mater.* **2017**, *27*, 1704092.
(41) Richards, C. I.; Choi, S.; Hsiang, J.-C.; Antoku, Y.; Vosch, T.; Bongiorno, A.; Tzeng, Y.-L.; Dickson, R. M. *J. Am. Chem. Soc.* **2008**, *130*, 5038−5039.
(42) Yeh, H.-C.; Sharma, J.; Han, J. J.; Martinez, J. S.; Werner, J. H. *Nano Lett.* **2010**, *10*, 3106−3110.
(43) Lu, C.-H.; Li, J.; Liu, J.-J.; Yang, H.-H.; Chen, X.; Chen, G.-N. *Chem. - Eur. J.* **2010**, *16*, 4889−4894.
(44) Liu, X. Q.; Wang, F.; Aizen, R.; Yehezkeli, O.; Willner, I. *J. Am. Chem. Soc.* **2013**, *135*, 11832−11839.
(45) Zhang, Y.; Zhu, C. F.; Zhang, L.; Tan, C. L.; Yang, J.; Chen, B.; Wang, L. H.; Zhang, H. *Small* **2015**, *11*, 1385−1389.
(46) Shi, Y.; Huang, W. T.; Luo, H. Q.; Li, N. B. *Chem. Commun.* **2011**, *47*, 4676−4678.
(47) Orbach, R.; Mostinski, L.; Wang, F.; Willner, I. *Chem. - Eur. J.* **2012**, *18*, 14689−14694.
(48) Chang, Y. Q.; Zhang, Z.; Liu, H. Q.; Wang, N.; Tang, J. L. *Analyst* **2016**, *141*, 4719−4724.

https://doi.org/10.1021/acs.analchem.1c03570
Anal. Chem. 2021, 93, 16025−16034